Progress In Electromagnetics Research B, Vol. 80, 19–36, 2018

Power Density Evaluation of a Novel Double-Stator Magnetic Geared Permanent Magnet Generator

Shehu M. Salihu[1], Norhisam Misron[1, 2, *], Mohammad L. Othman[1], and Tsuyoshi Hanamoto[3]

Abstract—This paper presents the power density evaluation and power mapping performance of a novel magnetic geared double-stator permanent magnet generator (DSPMG) which is proposed to address problems of mechanical geared generators for low-speed power generation applications. The operating principle is based on three PM rotors consisting of prime permanent-magnet (PM) poles in the middle rotor and field PM poles in the inner and outer rotors respectively. To evaluate the power density performance, a 2-D finite-element method (FEM) is used to predict the performance of the generator, and a demonstrator prototype is fabricated and evaluated experimentally. The power density characteristics of the proposed generator are analyzed and reported. The measured results agree closely with the simulated ones to verify the validity of the magnetic geared generator design. Finally, a measurable comparison is conducted with other published prototype magnetic gear machines to demonstrate its benefits of higher power density and smaller volume size.

1. INTRODUCTION

Research and development in magnetic gearing has attracted a lot of interest recently because of its potential for efficient transmission torque, lubrication free maintenance, overload protection and non-contact operation compared to mechanical gears that have problems of friction, wear and tear [1]. References [2, 3] reported that by integrating a magnetic gear with a PM machine, the resultant magnetic geared machine can be used as generators in low-speed renewable energy power generation applications. References [4, 5] reported in some studies that permanent magnet (PM) machines with a double-stator topology achieved greater performance characteristics than conventional single-stator permanent magnet machines. The research on magnetic geared double-stator PM machines has steadily increased recently in the last 10 years, although very few studies have been conducted on this class of MG machines. This could be as a result of the machine's complex structure which makes it difficult to manufacture and mechanically assemble. Jian and Chan [6] proposed a double-stator MG PM machine with its structure composed of two PM rotors and a single rotating modulating iron ring rotor. The magnetic geared machine was designed to operate in a motor/generator power-splitting mode for applications in electric vehicles (EVs). Liu et al. [7] proposed single-ring and dual-ring types of double-stator MG PM machine designs. Each MG PM machine consisted of a single PM rotor for low-speed, high torque applications. Niu et al. [8] presented an improved modified design by removing the modulating pole piece rotor and retaining two PM rotors. Non-magnetic ferrite poles were equally inserted between each pair of PMs to achieve a power-split electromechanical device (motor/generator). Wang et al. [9] published in a study

Received 23 October 2017, Accepted 10 February 2018, Scheduled 28 February 2018

* Corresponding author: Norhisam Misron (norhisam@upm.edu.my).

[1] Department of Electrical & Electronic, Faculty of Engineering, Universiti Putra Malaysia, UPM Serdang, Selangor 43400, Malaysia.

[2] Institute of Advanced Technology, Faculty of Engineering, Universiti Putra Malaysia, UPM Serdang, Selangor 43400, Malaysia.

[3] Department of Biological Functions Engineering, Graduate School of Life Science and Systems Engineering, Kyushu Institute of Technology, 2-4 Hibikino Wakamatsu-ku, Kitakyushu 808-0916, Japan.

two double-stator magnetic flux-modulated mnemonic machine designs that combined magnetic gearing principle and the concept of flux-mnemonic. The first machine design presented was a dual-layer PM magnetic flux-modulated mnemonic machine (MFMM) with PMs mounted on both the outer stator and rotor, while the second machine design proposed was a single layer PM magnetic flux-modulated mnemonic machine with all PMs fixed only on the outer stator.

Although previous reported studies conducted on MG double-stator PM machines have contributed significantly to the present knowledge about this class of magnetic geared machines, it can be reasonably assumed that the absence of published experimental data in [6–9] suggests that the performance characteristics of magnetic geared double-stator PM machines have not been fully studied and reported, to identify research areas requiring further investigation. One of these areas that this paper studies is power density evaluation of a double-stator magnetic geared PM generator, which has a novel structure that comprises three PM rotors and dual iron ring pole pieces integrated with two stators in a magnetically coupled configuration.

The purpose of this paper is to evaluate the power density performance of a magnetic geared double-stator PM generator with a novel structure from a prototype. The structure and operating principle of the generator based on the magnetic gear ratio is described in Section 2. Section 3 presents the finite element method. Section 4 presents the results and discussion. Finally, the conclusion is presented in Section 5.

2. MACHINE STRUCTURE AND OPERATING PRINCIPLE

Structure of the magnetic geared machine is shown in Figure 1. It consists of three PM rotors, two iron ring pole pieces and two stators. The prime PMs are fixed on the middle rotor to form the prime mover, while field PMs are mounted on both outer and inner rotors. A mutually magnetically coupled configuration is used to integrate the magnetic gear with the PM machine, resulting in magnetic gearing and electrical power generation simultaneously. A double-layer concentrated winding topology as shown in Figure 3 is used to connect the machine. The mechanical assembly of the magnetic geared generator is illustrated in Figure 4, and it can be observed that the three PM rotors rotate independently in the axial direction. Also to reduce the cost and quantity of PMs, a bone rotor structure is implemented in the machine design. When the low-speed prime PM rotor rotates, both outer and inner field PM rotors revolve synchronously opposite in direction to the prime rotor according to the gear ratio. The field PM rotors induce excitation in the coil windings to produce an EMF, resulting in electrical power generation. The design specifications of the magnetic geared generator are listed in Table 1 while material properties of the machine parts and winding specifications are given in Table 2.

For the magnetic gear ratio design, the numbers of pole pairs selected for the low-speed prime PMs

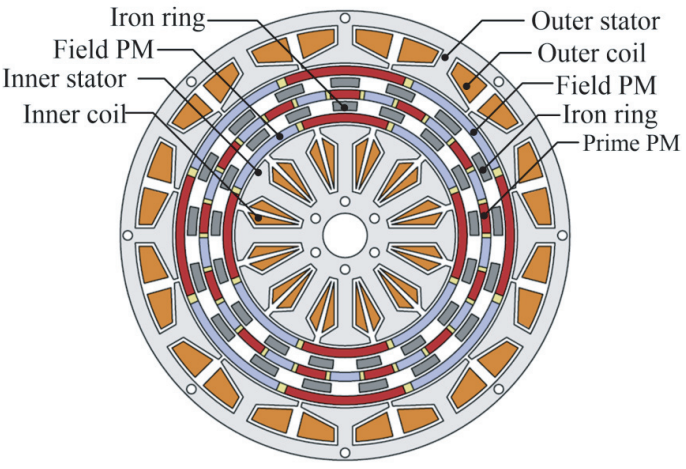

Figure 1. Double-stator PM generator integrated with magnetic gear.

and high-speed field PMs are 13 and 4, respectively. From the gear ratio map shown in Figure 2, this pole pair combination produces a gear ratio of 3.25 and a cogging torque factor of $C_f = 1$ as defined by [10] and C_f is expressed as

$$C_f = \frac{2P_{field}N_{iron}}{LCM(2P_{field}N_{iron})} \tag{1}$$

where P_{field} is the number of poles on the high-speed field PM rotor, N_{iron} the number of stationary iron pole pieces, and LCM the smallest common multiple between the number of high-speed field PMs and number of stationary iron pole pieces. The magnetic flux modulation between 13 pole pair low-speed

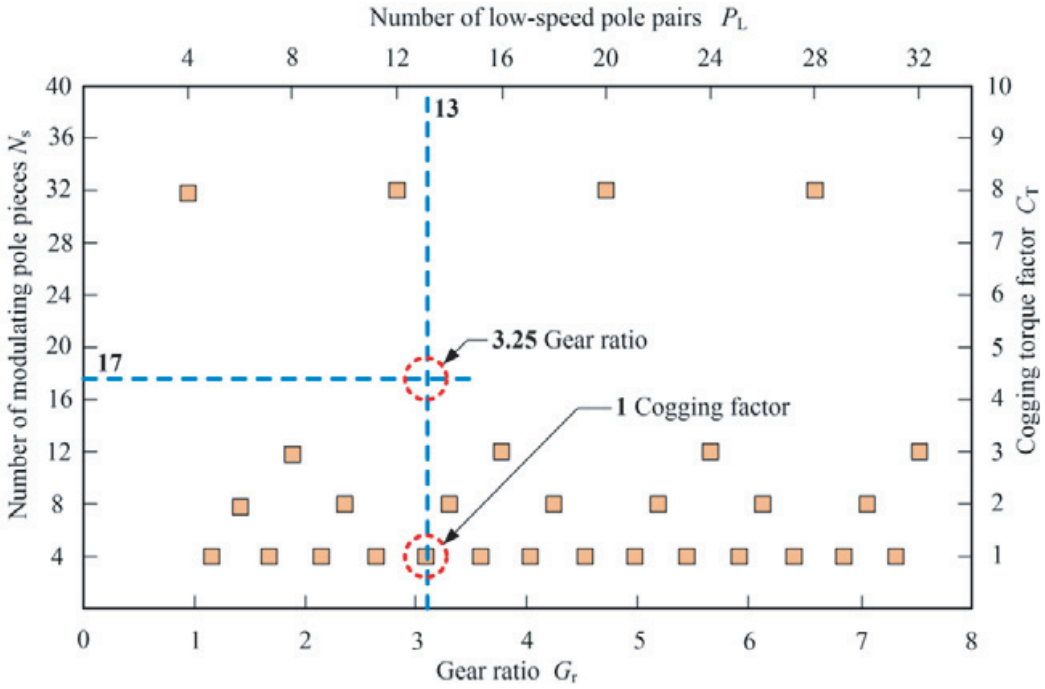

Figure 2. Gear ratio map.

Table 1. Design specifications of the proposed MG machine.

Parameter	Dimension
Outer and inner airgap lengths	1.0 mm
Outer stator outside diameter	150 mm
Outer stator inside diameter	116.6 mm
Inner stator outside diameter	74.6 mm
Inner stator inside diameter	14.0 mm
Axial length	30.0 mm
No. of outer and inner stator slots	12
No. of outer and inner field PMs	8
No. of prime PMs	26
No. of outer and inner pole pieces	17
No. of phases	3
Cogging torque factor	1
Magnetic gear ratio	3.25

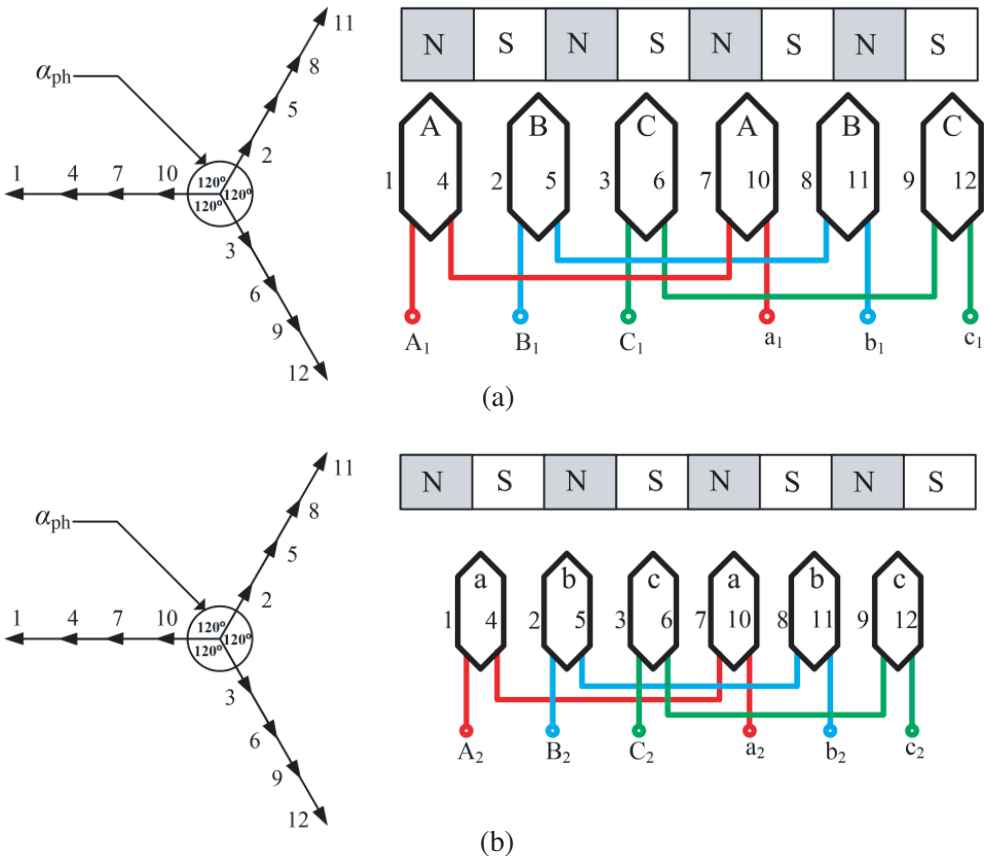

Figure 3. Winding diagram layout for the MG machine. (a) Outer stator. (b) Inner stator.

Table 2. Property of materials and winding specifications.

Component	Material
Magnets	Nd-Fe-B-38H
Pole pieces	SS400
Rotors	SS400
Stators	50H800 Laminated steel
Diameter of wire	0.80 mm
Number of turns outer coil	75
Number of turns inner coil	31
Resistance per phase outer coil	1.70 Ω
Resistance per phase inner coil	0.80 Ω
Phase connection	Star

prime PMs and 4 pole pair high-speed field PMs governs the transmission torque of the magnetic gear. According to the magnetic gearing principle [11], the magnetic gear relationship between the rotational speed ratio of the number of pole-pairs and the airgap flux density space harmonics is governed by

$$\omega_{\text{prime}} = \frac{p_{\text{prime}}}{|p_{\text{prime}} - p_{\text{iron}}|}\omega_{\text{field}} + \frac{p_{\text{iron}}}{|p_{\text{iron}} - p_{\text{prime}}|}\omega_{\text{iron}} \tag{2}$$

$$p_{\text{field}} = |p_{\text{iron}} - p_{\text{prime}}| \tag{3}$$

where ω_{field}, ω_{prime}, and ω_{iron} are the rotational speeds of the high-speed field PM rotor, low-speed prime PM rotor and stationary iron pole pieces respectively while p_{prime}, p_{field}, and p_{iron} are the pole pair number of low-speed prime PMs, high-speed field PMs and number of stationary iron pole pieces, respectively. The magnetic gear ratio G_{r} can be expressed as

$$G_{\text{r}} = -\frac{\omega_{\text{prime}}}{\omega_{\text{field}}}\bigg|_{\omega_{\text{iron}}=0} = \frac{p_{\text{prime}}}{p_{\text{field}}} \tag{4}$$

therefore a gear ratio of 3.25 is computed for the MG generator, and the minus sign indicates that both inner and outer high-speed field PM rotors rotate simultaneously opposite in direction to the low-speed prime PM rotor. The number of slots per pole per phase $q = 1/2$ is a fractional number; therefore, a 3-phase concentrated winding topology shown in Figure 3 is adopted for the MG generator as this design can reduce copper losses [12].

2.1. Mechanical Assembly

A magnetically coupled configuration is realized for the whole MG machine as shown in Figure 4 by integrating the magnetic gear with a double-stator PM machine. The PMs are placed between three rotors, and a bone rotor structure is used to reduce the quantity of PMs to three layers. This design enables the input shaft which functions as the prime mover to be coupled to the prime PM rotor while outer and inner field PM rotors rotate simultaneously at the same speed opposite in direction to the prime PM rotor. The prime PM rotor can couple or decouple both outer and inner field PM rotors by slipping if maximum torque and ohmic load is exceeded by slipping. The pole pieces are manufactured from solid steel of 3 mm thickness. Although laminated steel would have been a better option to reduce losses from eddy currents, manufacturing cost and complexities in the mechanical assembly were considered. The three PM rotors and steel pole pieces are supported on both ends with aluminium end rings to reduce magnetic flux leakage in the axial direction and short circuiting of the pole pieces.

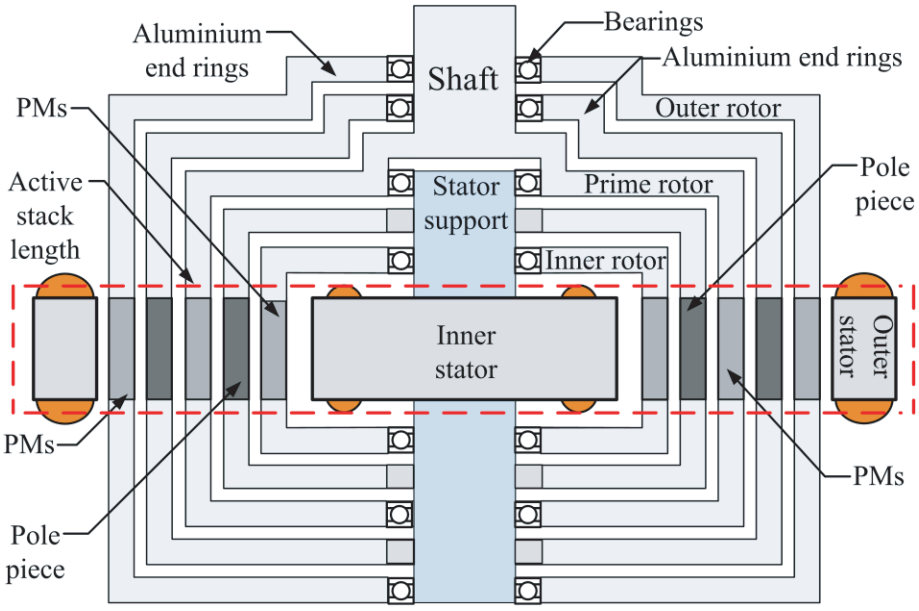

Figure 4. A 2D concept mechanical assembly of the prototype.

2.2. Power Density and Active Volume Evaluation

If a purely ohmic load is connected to an AC power generator in a balanced three-phase wye configuration, the AC current flowing through each ohmic load will vary simultaneously with the AC voltage. For a balanced three-phase wye connected resistive load, the active power P_{active} dissipated

by the generator is the sum of the average real power, $\mathbf{P_{active}=3V_{rms}I_{rms}PF}$ where $V_{\rm rms}$ is the rms value of the AC voltage, $I_{\rm rms}$ the rms value of the AC current, and PF the power factor of the magnetic geared generator. The MG generator power density $P_{\rm density}$ for the total active volume can be obtained as

$$P_{density} = \frac{P_{\rm max}}{V_{active}} \tag{5}$$

where $P_{\rm max}$ and $V_{\rm active}$ are the maximum output electrical power and active volumetric density of the MG generator. The overall active volume of the MG machine can be calculated based on the active stack length from various materials used such as PMs, steel pole pieces, steel rotors and laminated stator cores. Aluminium material is used for end connecting rings on the three PM rotors and two iron pole pieces to reduce leakage flux. End connecting rings are not considered in calculating the active volume of the MG machine, for the reason that aluminium is a magnetic flux barrier. A computer aided design software tool is used to calculate the volume of the solid active components from a a 3D model of the prototype as shown in Figure 5, and the estimated volumes are summarized in Table 3.

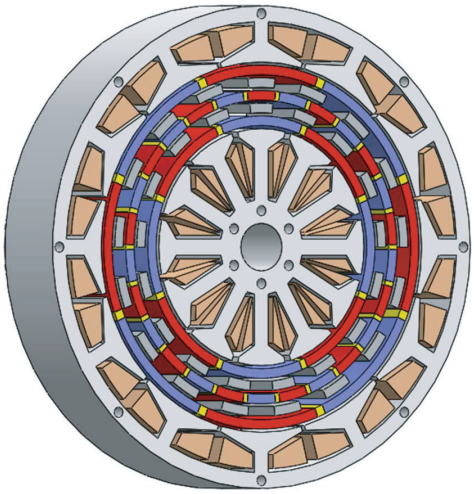

Figure 5. A 3D model of the prototype for estimation of active volume.

Table 3. The estimated active volume of the magnetic geared machine.

Magnetic Geared Double-Stator PM Generator		
	Component	**Volume size [cm^3]**
Active stack length [30 mm]	Outer stator	124.65
	Inner stator	74.11
	Outer field PMs	29.45
	Inner field PMs	21.01
	Prime PMs	23.43
	Outer pole pieces	14.65
	Inner pole pieces	12.38
	Outer rotor	2.10
	Inner rotor	1.50
	Prime rotor	3.60
	Outer coil*	63.67
	Inner coil*	22.04
	Total size	393

*Excluding coil end-winding.

3. FINITE ELEMENT METHOD

A two-dimension finite element method (2D-FEM) numerical tool is used to evaluate performance characteristics of the proposed machine. To predict electromagnetic characteristics of the MG generator, a transient response simulation analysis was conducted by modelling a 2D FEM model of the MG machine using two-dimensional finite element method. The MG generator is not symmetrical; therefore, the absence of periodicity requires a full 2D model to be constructed. Although 3D FEM would have been more suitable to accurately predict other performance characteristics of the MG generator such as magnetic flux or end effects in the axial direction, due to the limitation of the research, these properties are not within the scope of this study as 3D FEM is computer hardware and time intensive. The MG machine has several air-gaps (six in number) and will require the finest mesh for accurate simulated results as there will be large variation of the magnetic flux densities in the air-gaps. There is no boundary element created between the machine model and non-modeled region in the boundary region. Also the machine model consists of magnetic materials, hence electromagnetic forces on the magnets are concentrated at the nearest nodes. For these reasons, nodal force method is selected as the calculation method for 2D FEM simulation. The 2D finite element analysis and magnetic flux plot of the magnetic geared generator are shown in Figure 6, and it is observed that the flux lines crossing across the airgap enable flux linkage between the magnetic gear and generator in the magnetically coupled configuration. It demonstrates that integration of the magnetic gear with a double-stator PM machine is achieved with the proposed design.

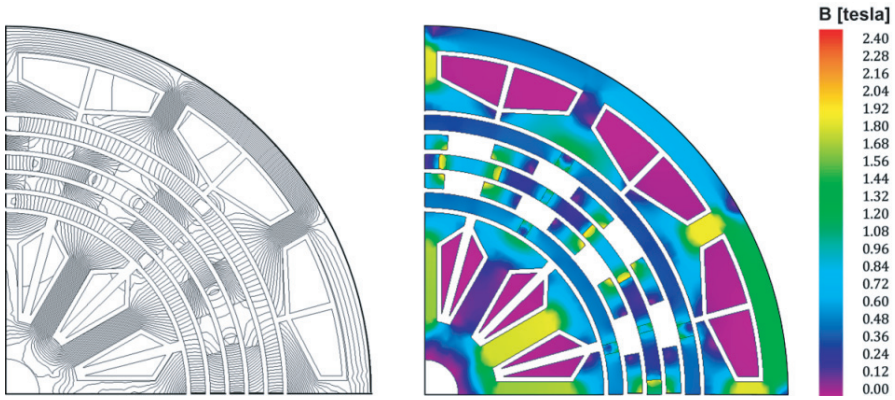

Figure 6. Flux density distribution and flux lines.

4. RESULTS AND DISCUSSION

4.1. Transient Response Analysis

The transient losses in the PMs are estimated in the 2D FEM simulation by modeling each magnet as a conductor with its respective material resistivity, while the losses in the modulating pole pieces are calculated by modeling the pole pieces similar to bars in a squirrel cage rotor [13, 14]. A 3D FEM would have been better for computing the losses due to eddy current in the end rings and pole pieces. However, 3D finite element analysis is time consuming and computationally expensive. The eddy current losses in the PMs and pole pieces are shown as a function of time for various prime speeds in Figure 7. It can be observed that with increase in prime rotor speed, the losses due to eddy currents are greater. In Figure 7(a) at prime rotor speed of 100 rpm, the losses in the PMs and pole pieces are 7 W and 46 W, respectively, while in Figure 7(b) at prime rotor speed of 300 rpm, the losses in the PMs and pole pieces are 61 W and 384 W, respectively. In Figure 7(c) at prime rotor speed of 500 rpm, the losses are 157 W and 989 W for the PMs and pole pieces, respectively. It can be concluded that the losses are primarily produced in the pole pieces due eddy currents resulting from the use of solid instead of laminated steel.

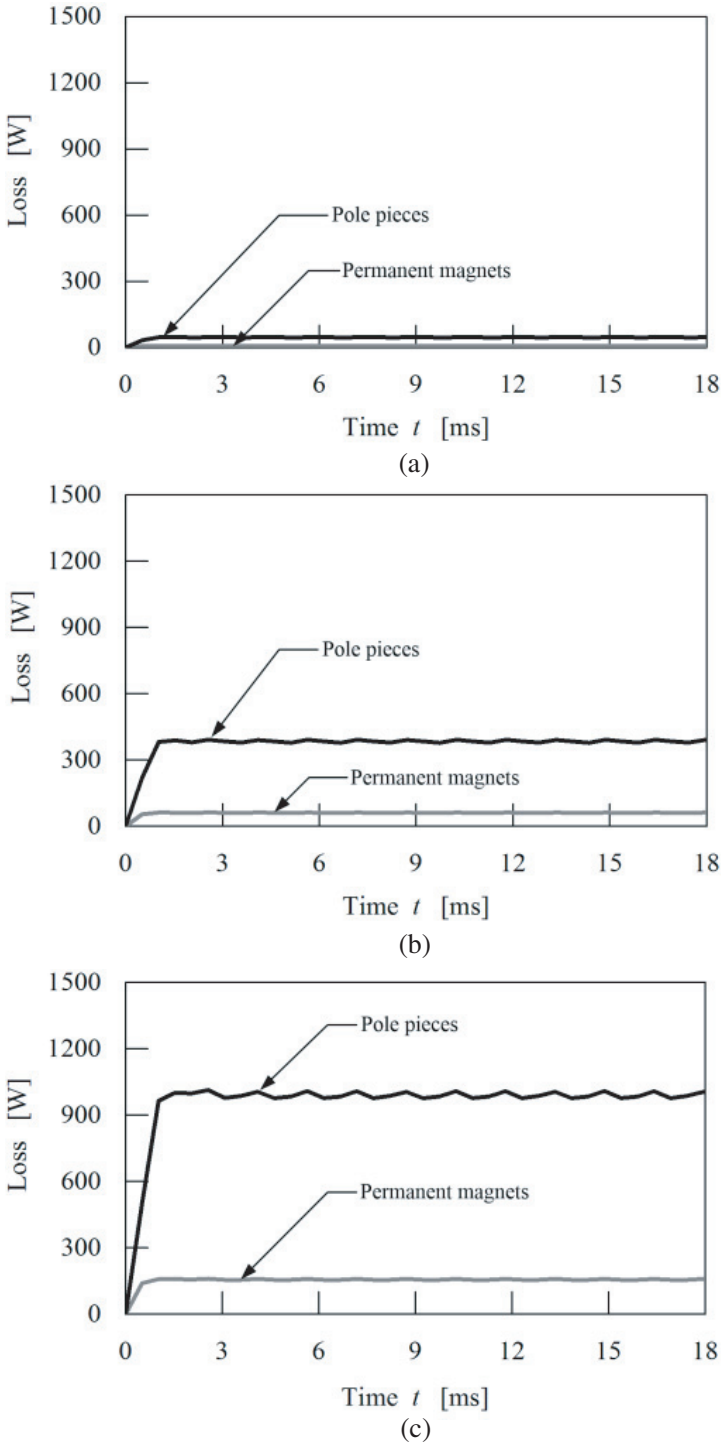

Figure 7. Pole pieces and permanent magnets losses with ohmic load of 31 Ω at various prime rotor speeds. (a) Prime speed = 100 rpm. (b) Prime speed = 300 rpm. (c) Prime speed = 500 rpm.

The core and copper losses as a function of resistive load for various prime rotor speeds are shown in Figure 8, and it can be seen that the losses increase with corresponding increase in prime rotor speed. In Figure 8(a) when the generator's prime rotor speed is 100 rpm, 300 rpm and 500 rpm, the core losses are 3 W, 12 W and 24 W, respectively, while the copper losses shown in Figure 8(b) are 2 W, 11 W and 26 W, respectively. The total losses (core loss + copper loss) as shown in Figure 8(c) at prime rotor

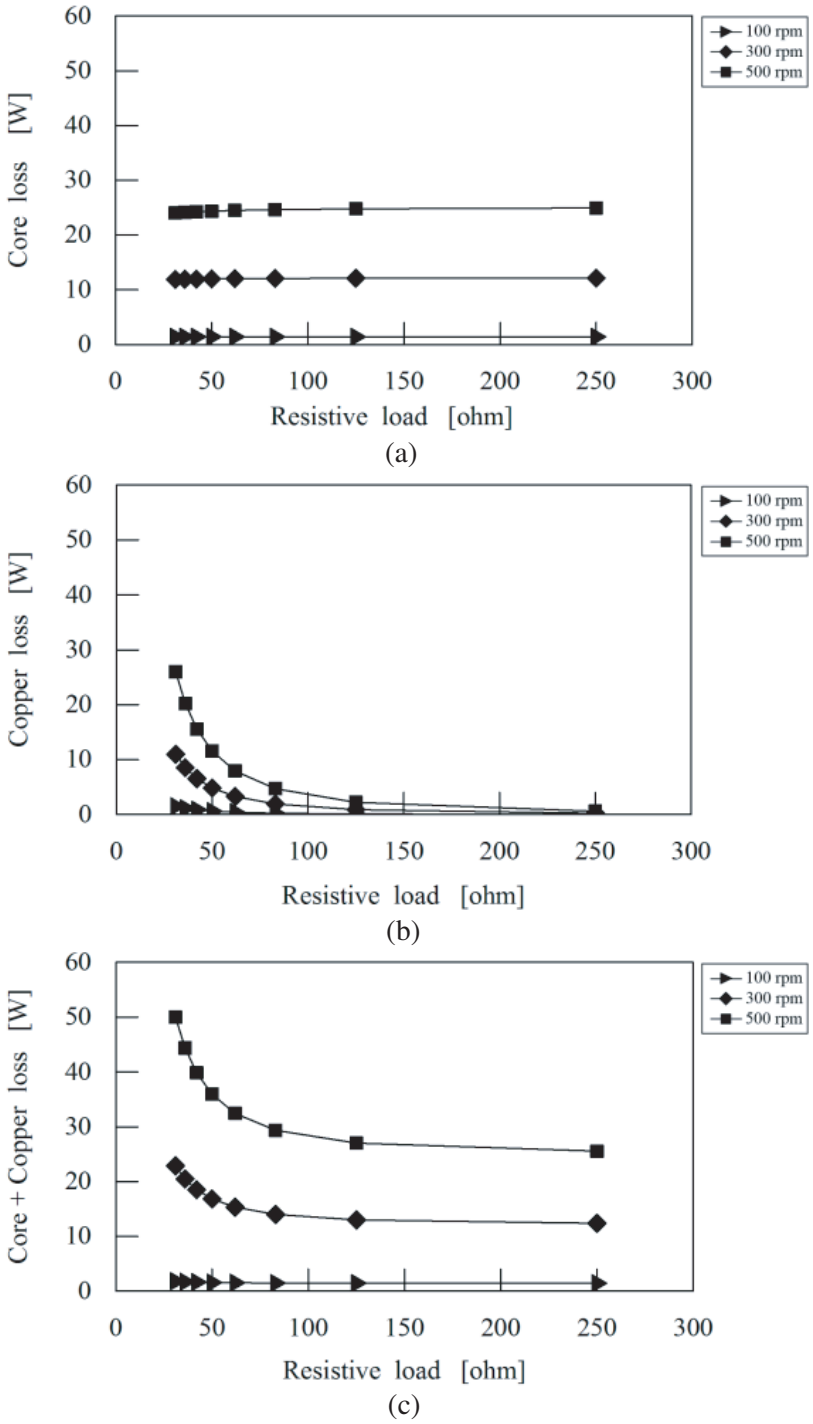

Figure 8. Core and copper losses at various prime rotor speeds. (a) Core losses. (b) Copper losses. (c) Core and copper losses.

speed of 100 rpm, 300 rpm and 500 rpm are 5 W, 23 W and 50 W respectively. At greater prime rotor speed, variation of the magnetic flux increases to produce higher copper and core losses in the coil windings and stator core, respectively. The PMs and pole piece losses as a function of resistive load are presented in Figure 9(a) and Figure 9(b). It can be seen that the losses also increase at higher prime rotor speed due to changes in the magnetic flux. The losses from the PMs at prime rotor speeds of

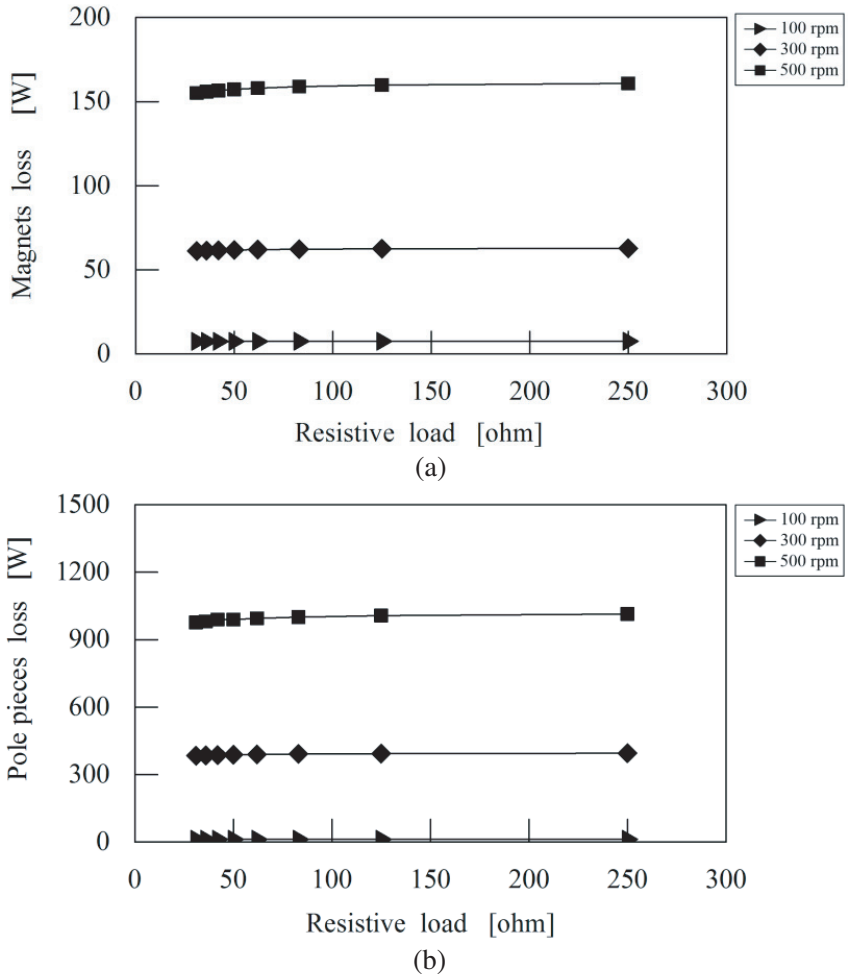

Figure 9. Permanent magnets and pole piece losses at various prime rotor speeds. (a) Permanent magnets losses. (b) Pole piece losses.

100 rpm, 300 rpm and 500 rpm are 7 W, 61 W and 155 W respectively, while losses from the pole pieces are 47 W, 384 W and 976 W, respectively. The transient analysis shows that losses are mainly produced in steel pole pieces as a result of high eddy currents which could reduce the maximum transmission torque of the generator, therefore resulting in slipping and decoupling of the magnetic gear from the generator.

4.2. Prototype Assembly

A 2D frontal view of the assembled magnetic geared generator is shown in Figure 10. The three PM rotors revolve independently on the same axis therefore resulting in mechanical difficulties in the assembly due to manufacturing tolerances of the machine components. Also when the ferromagnetic pole pieces are inserted between the field PMs and prime PMs, the difficulty in the mechanical assembly increases because the pole pieces are pulled on both sides by strong magnetic forces from the PMs. Both ferromagnetic pole pieces are machined from solid steel rather than laminated sheets due to cost considerations and ease of assembly. The field and prime PMs have equal dimension of 3 mm thickness similar to the three rotors. In order to protect the PMs from centrifugal forces at high speeds, aluminium end rings are secured on each end of the PM rotors. Though eddy current loops exist between the aluminium end rings and ferromagnetic pole pieces, the scope of this research is aimed for low-speed power generation. Therefore, this factor is ignored. As observed in Figure 10, a magnetically coupled configuration is achieved by the integration of the PM generator and magnetic gear.

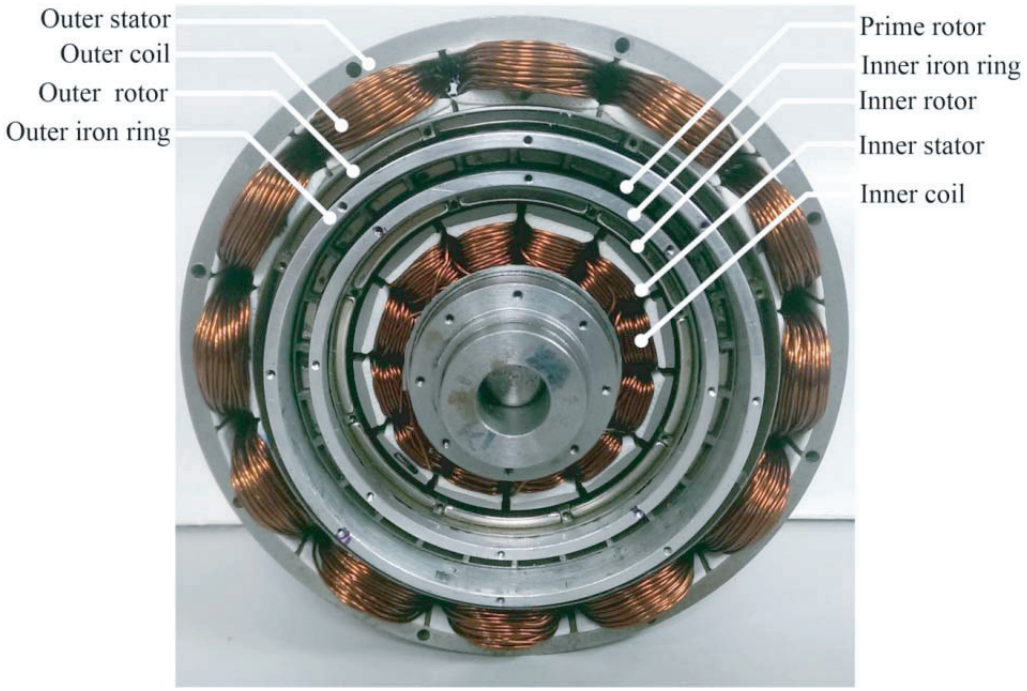

Figure 10. Prototype assembly of magnetic geared generator.

4.3. Measurement Setup

A block diagram and an experimental setup for measuring the active AC power dissipated by the generator are shown in Figure 11(a) and Figure 11(b), respectively. The MG generator was connected to a balanced three phase resistor load bank in wye configuration while the AC power was measured with a Hioki power analyzer. The three-phase resistor load bank is configured with a minimum ohmic load of 31 ohm per phase and a maximum ohmic load of 250 ohm per phase. The resistor load bank is electrically isolated from the MG generator with a three-phase circuit breaker switch and is closed to electrically load the MG generator. The circuit breaker switch is opened before varying the resistor load bank. At constant prime rotor speed, the torque, speed and electrical power are measured and recorded. It was observed that the output AC voltage and AC current waveform shapes produced by the prototype MG generator were non-sinusoidal. However, true rms values are valid only if waveforms are purely sinusoidal in shape. The power analyzer converts the non-sinusoidal voltage and current rms to true rms value V_{rms} with the following equation given by

$$V_{\text{rms}}=\sqrt{\frac{1}{S}\left(V_1^2+V_2^2+V_3^2+\ldots+V_{\text{s}}^2\right)} \tag{6}$$

where S is the number of samples recorded in one period.

4.4. On-Load and Back EMF Voltage Characteristics

By connecting an ohmic load of 62 ohm per phase at constant prime rotor speed of 200 rpm, the simulated and measured voltage, current waveforms are shown in Figures 12(a) and 12(b). It can be observed that the phase-to-neutral voltage waveforms V_{a}, V_{b} and V_{c} are balanced, and the results are in good agreement. The AC voltage and AC current waveforms are equally in phase which is normal for a purely ohmic load. The peak phase voltages from the calculated and measured results are ≈ 42 V and ≈ 42 V, while the calculated and measured peak phase currents are ≈ 0.69 A and ≈ 0.66 A, respectively. It can be observed that third-harmonics are dominant in phase voltage and phase current waveforms which are a general feature with concentrated windings and the pole-slot selection. The simulated and measured no-load back EMF waveforms of the MG generator are compared in Figure 12(c). It can be seen that

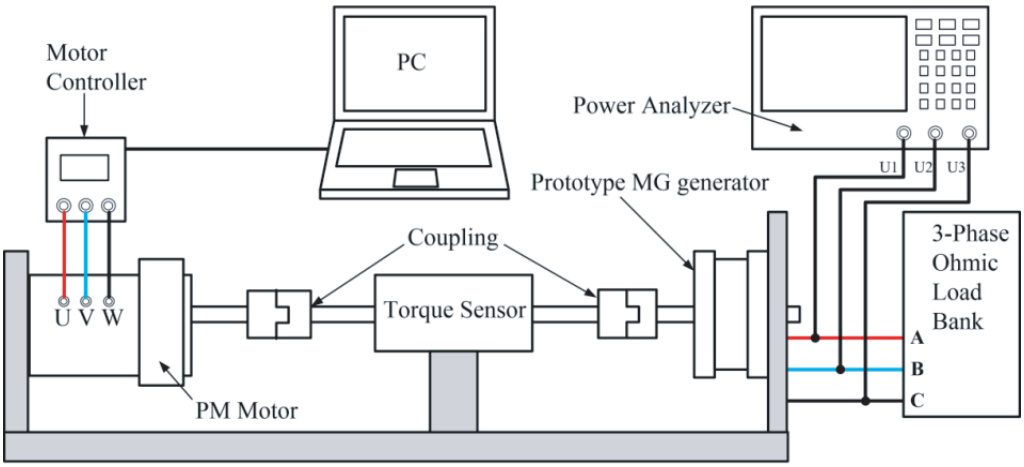

(a)

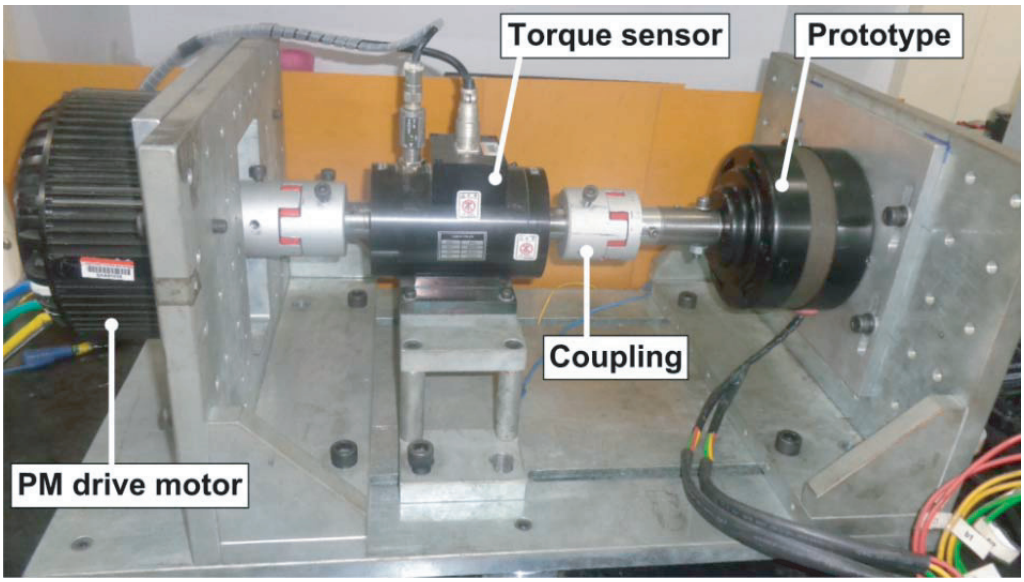

(b)

Figure 11. Measurement setup. (a) AC power measurement block diagram. (b) Test rig with prototype.

the two waveforms are similar in shape, though the simulated result is greater in amplitude than the measured result. Therefore line-to-line voltage can improve distortion of its waveform to generate a nearly sinusoidal waveform shape by reducing the effect of third harmonics. Also a distributed winding configuration and selecting a specific slot pole combination are other methods that can be used to reduce the generator voltage distortions.

4.5. Torque, Power and Efficiency Characteristics

The torque as a function of prime rotor speed characteristics for the MG generator is shown in Figure 13(a), and the maximum torque achieved by the MG generator is $\approx$ 11 Nm with ohmic load per phase of 83 ohm at prime rotor speed of 425 rpm. At constant ohmic load per phase, torque increases linearly with increase in prime rotor speed while a decrease in ohmic load per phase results in increase in torque. When ohmic load is reduced, the output current increases which results in increase in counter torque from the MG generator. To balance this counter torque, the input torque on the prime mover is increased. The total measured three-phase active power dissipated by the MG generator

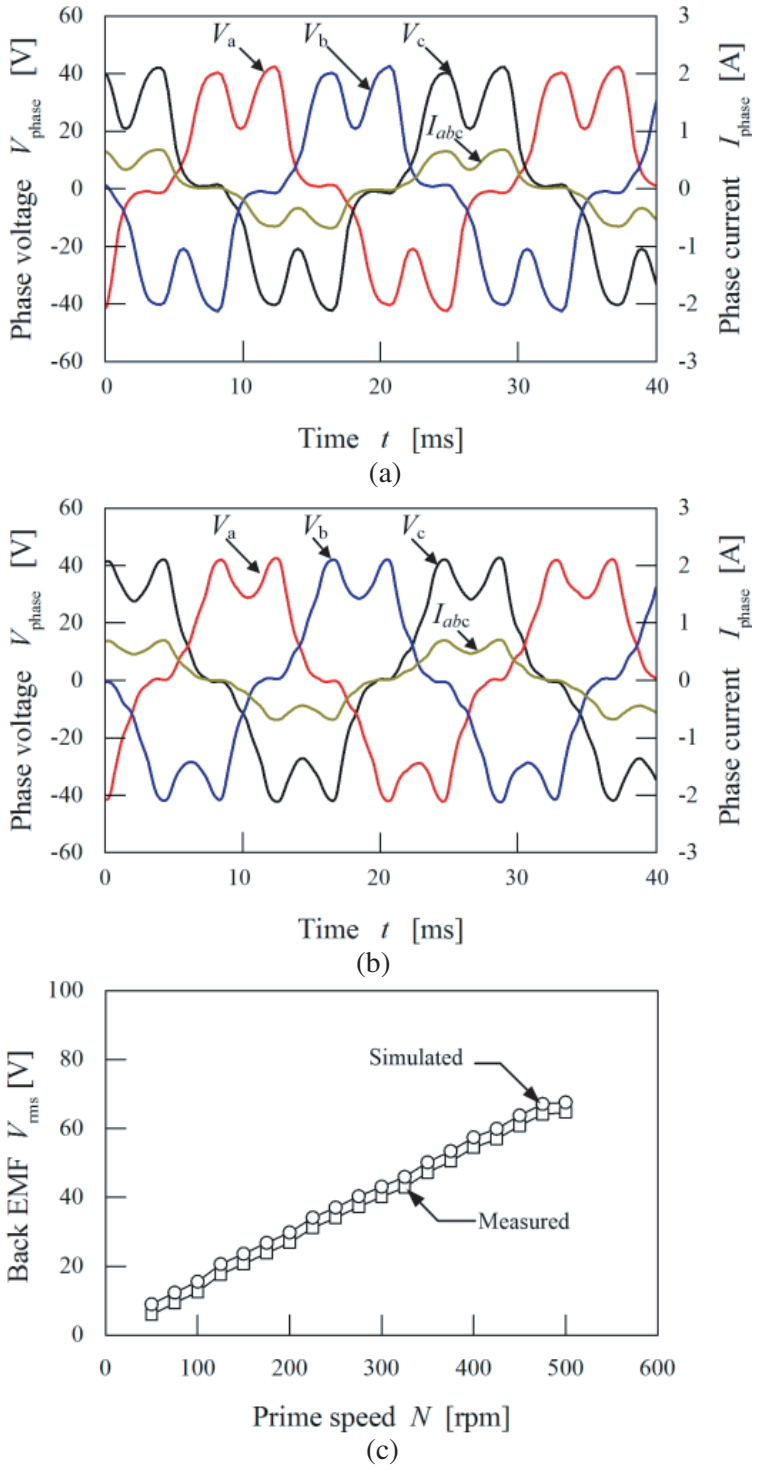

Figure 12. On-load and back EMF characteristics. (a) Simulated on-load waveform. (b) Measured on-load waveform. (c) Comparison of no-load voltage as function of prime rotor speed.

is shown in Figure 13(b). The total maximum active AC power dissipated by the generator is ≈ 360 W at prime rotor speed of 500 rpm with resistive load per phase of 31 ohm. It can be observed that when ohmic load per phase increases, the maximum active AC power drops despite an increase in prime rotor speed. This can be explained by the fact that the MG generator has reached its maximum operating

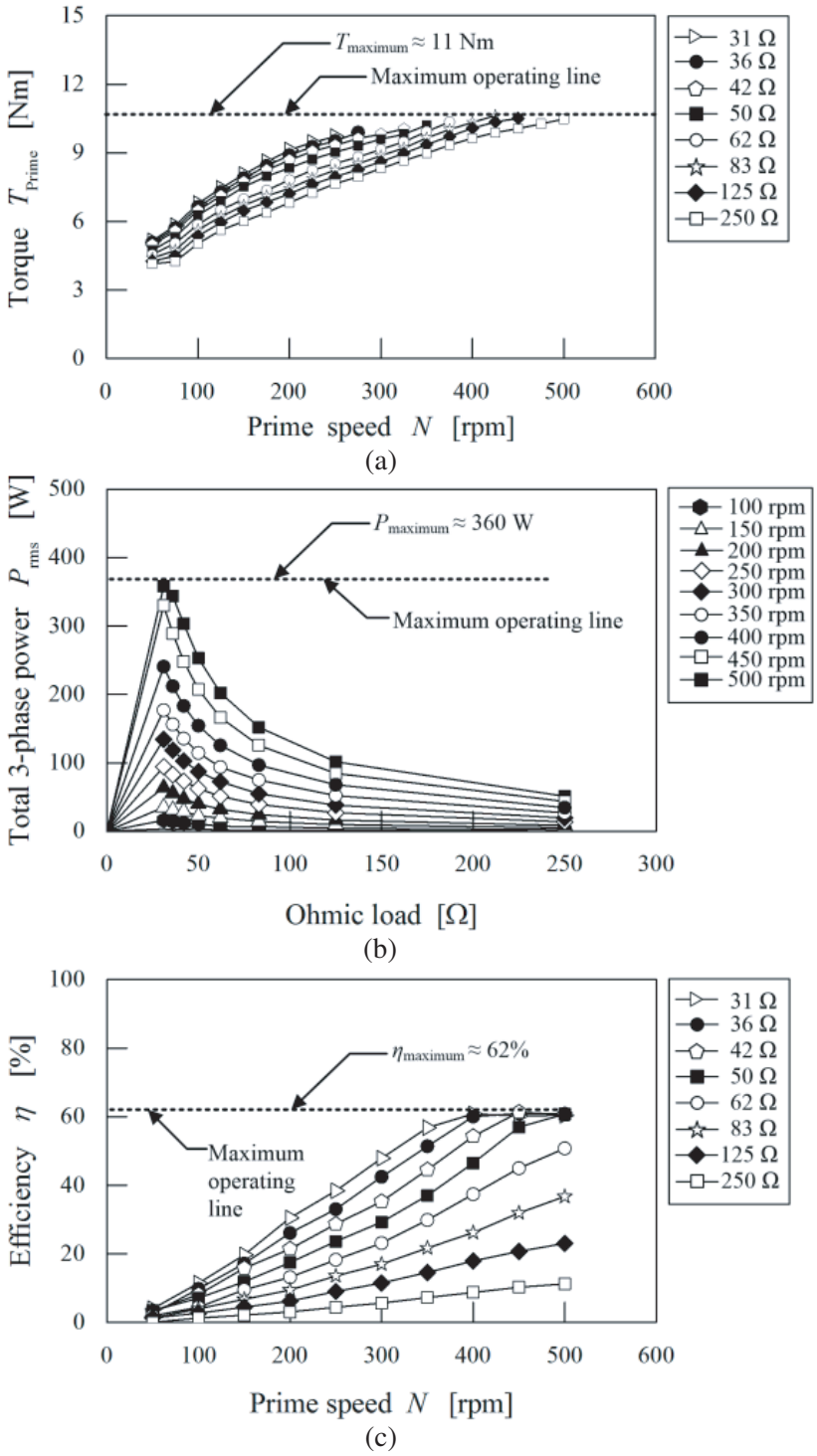

Figure 13. Torque, power and efficiency characteristics. (a) Torque as function of prime speed. (b) Power as function of ohmic load. (c) Efficiency as function of prime speed.

point as a result of saturation and impedance matching. Also the maximum prime rotor speed of the MG generator that generates active AC power before it slips is 500 rpm. As shown in Figure 13(c), the maximum efficiency achieved by the MG generator is $\approx 62\%$ with ohmic load of 42 ohm at 450 rpm.

4.6. Power Density and Power Mapping Characteristics

The active power density as a function of ohmic load is shown in Figure 14(a), and the maximum power density achieved by the MG generator is $\approx 917\,\mathrm{kW/m^3}$ at prime rotor speed of 500 rpm. It can be observed from the power density curve that the peak point of saturation is reached when ohmic load

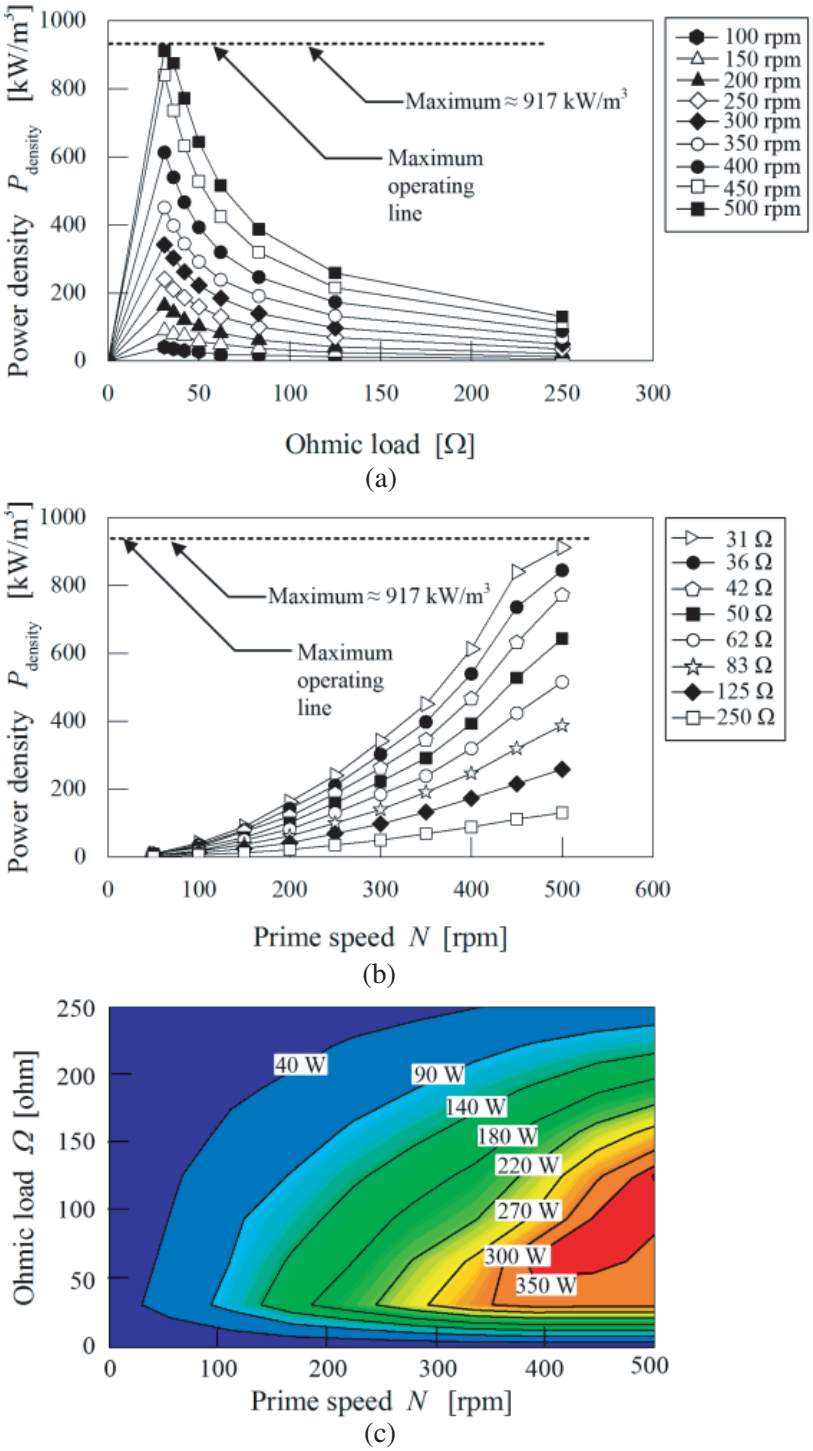

Figure 14. Power density and power mapping characteristics. (a) Power density as function of ohmic load. (b) Power density as function of prime speed. (c) Power mapping as function of ohmic load and prime speed.

is 31 ohm per phase, and the curve decreases with increase in prime rotor speed. Similarly, the active power density as a function of prime rotor speed is shown in Figure 14(b), and maximum active power density is achieved at prime rotor speed of 500 rpm with ohmic load of 31 ohm per phase. The results show that with an active volumetric density of $\approx 393\,\mathrm{cm}^3$ the MG generator can achieve a high power density for its volume size. The power mapping characteristic of the MG generator as illustrated in Figure 14(c) is measured at various ohmic load and operating speeds. It can be observed that power increases proportionally with increase in prime rotor speed at constant ohmic load. Power mapping of the MG generator demonstrates that when ohmic load is constant with variable prime rotor speed, the power dissipation increases until a peak point of saturation is reached. When ohmic load is less than 50 ohm per phase, maximum active power is dissipated by the MG generator, and when ohmic load is increased, the output electrical power decreases because the ohmic load is approximately equal to the generator's internal resistance. This demonstrates that by varying the ohmic load resistance on the MG generator, maximum active power is achieved by impedance matching of both ohmic load and MG generator's internal resistance.

4.7. Comparison of Proposed MG Generator with Published Prototype Machines

A measurable comparison of the proposed MG generator with some published prototypes to establish the benefits of high power to low volumetric density ratio is listed in Table 4. However, it should be noted that the comparison is primarily to demonstrate that the proposed MG generator can achieve equal or greater power density with a smaller machine size than other MG generators. From the reported studies conducted, only the active stack length excluding the outer casing of the prototypes is used to estimate the volume sizes of the magnetic gear and generator parts. It can be observed in Table 4 that the proposed MG generator is the least in volume size, output power and stack length but greatest in power density. Also the torque densities of machines C, D and the proposed MG generator indicate their suitability for low-speed high torque applications. Though machine model D is the smallest in diameter with high torque density, it is superseded 13% in power density by the proposed MG generator. The power density as a function of machine size for some published prototypes is compared with the proposed MG generator and shown in Figure 15. It can be observed that machine model A exhibits the largest diameter and lowest power density, while the proposed MG generator is characterized with the highest power density. Based on the graphical data shown in Figure 15, the proposed MG generator is advantageous with smaller volume size and higher power density than other published prototype machine models.

Table 4. Measurable comparison of proposed MG generator with reported prototypes.

Parameter	**[2]**	**[15]**	**[16]**	**[17]**	**Proposed**
	A	**B**	**C**	**D**	
Generator prototype	Single stator axial flux	Single stator axial flux	Single stator radial flux	Single stator radial flux	Double stator radial flux
Gear ratio	9.33	6.67	7.33	10.5	3.25
Active volume* [cm^3]	5410	20753	1064	602	393
Outer diameter [mm]	260	250	184	140	150
Active stack length [mm]	76.2	58.8	40	50	30
Power [W]	1000	4000	500	488	360
Torque density† [$\mathrm{kNm/m}^3$]	7.8	9.3	70	68.6	27.9
Power density* [$\mathrm{kW/m}^3$]	185	192	469	811	917

*Excluding outer casing considering only active volume.
†The overall machine including generator and magnetic gear minus outer casing.

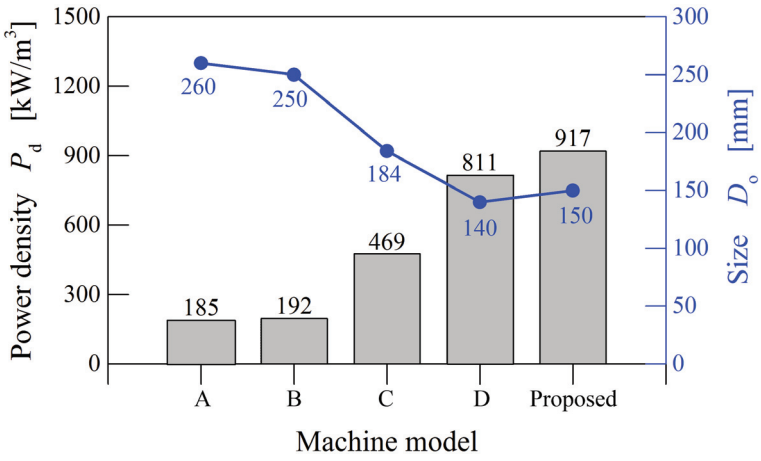

Figure 15. The power density as a function of size for each machine model.

5. CONCLUSION

The power density of a novel magnetic geared double-stator PM generator has been evaluated and reported in this study. Power density characteristics have been measured from a constructed prototype. This study found that with an active volumetric density of $\approx 393\,\text{cm}^3$ the MG generator demonstrated a maximum active power density of $\approx 917\,\text{kW/m}^3$ for various ohmic loads at variable prime rotor speed. Also the maximum measured efficiency achieved by the MG generator was $\approx 62\%$ at maximum prime speed of 500 rpm. The maximum prime speed of the MG machine for inherent overload protection is 500 rpm, which is consistent with magnetic gears and an advantage for low-speed renewable energy applications. The power mapping characteristics showed that power increases proportionally with increase in prime rotor speed at constant ohmic load while maximum active power is dissipated by the MG generator when ohmic load is less than 50 ohm per phase. Finally, a measurable comparison with some published prototype MG machines has demonstrated that the proposed MG generator with a double-stator structure can achieve greater power density with a reduced volume size than other prototype single-stator MG PM generators. As can be observed, a measured power density of $\approx 917\,\text{kW/m}^3$ which is similar to or greater than that of single-stator magnetic geared PM generators, can be achieved by integrating a conventional double-stator PM generator with a magnetic gear. It has also been demonstrated that the structure and size of the MG generator influence the power to volume ratio and that a power density can be achieved which is comparable to or better than single-stator MG generators when a magnetic gear is integrated with a conventional double-stator PM machine.

REFERENCES

1. Li, X., K. Chau, M. Cheng, and W. Hua, "Comparison of magnetic-geared permanent-magnet machines," *Progress In Electromagnetics Research*, Vol. 133, 177–198, 2013.
2. Johnson, M., M. Gardner, and H. Toliyat, "Design and analysis of an axial flux magnetically geared generator," *IEEE Transactions on Industry Applications*, Vol. 53, No. 1, 97–105, 2017.
3. Oshiumi, T., N. Niguchi and K. Hirata, "Experiment of 1 kW class magnetic-geared generator," *Journal of the Japan Society of Applied Electromagnetics and Mechanics*, Vol. 22, No. 2, 183–188, 2014.
4. Niu, S., K. Chau, J. Jiang, and C. Liu, "Design and control of a new double-stator cup-rotor permanent-magnet machine for wind power generation," *IEEE Transactions on Magnetics*, Vol. 43, No. 6, 2501–2503, 2007.
5. Niu, S., K. Chau, and C. Yu, "Quantitative comparison of double-stator and traditional permanent magnet brushless machines," *Journal of Applied Physics*, Vol. 105, No. 7, 07F105, 2009.

6. Jian, L. and K. Chau, "Design and analysis of a magnetic-geared electronic-continuously variable transmission system using finite element method," *Progress In Electromagnetics Research*, Vol. 107, 47–61, 2010.
7. Liu, C., K. Chau, and Z. Zhang, "Novel design of double-stator single-rotor magnetic-geared machines," *IEEE Transactions on Magnetics*, Vol. 48, No. 11, 4180–4183, 2012.
8. Niu, S., S. Ho, and W. Fu, "A novel double-stator double-rotor brushless electrical continuously variable transmission system," *IEEE Transactions on Magnetics*, Vol. 49, No. 7, 3909–3912, 2013.
9. Wang, Q., S. Niu, S. Ho, W. Fu, and S. Zuo, "Design and analysis of novel magnetic flux-modulated mnemonic machines," *IET Electric Power Applications*, Vol. 9, No. 7, 469–477, 2015.
10. Zhu, Z. and D. Howe, "Influence of design parameters on cogging torque in permanent magnet machines," *IEEE Transactions on Energy Conversion*, Vol. 15, No. 4, 407–412, 2000.
11. Atallah, K. and D. Howe, "A novel high-performance magnetic gear," *IEEE Transactions on Magnetics*, Vol. 37, No. 4, 2844–2846, 2001.
12. El-Refaie, A., "Fractional-slot concentrated-windings synchronous permanent magnet machines: Opportunities and challenges," *IEEE Transactions on Industrial Electronics*, Vol. 57, No. 1, 107–121, 2010.
13. Ishikawa, T., S. Shinagawa, and N. Kurita, "Analysis and failure diagnosis of squirrel-cage induction motor with broken rotor bars and end rings," *IEEJ Journal of Industry Applications*, Vol. 2, No. 6, 292–297, 2013.
14. Hanafy, H., T. Abdo, and A. Adly, "2D finite element analysis and force calculations for induction motors with broken bars," *Ain Shams Engineering Journal*, Vol. 5, No. 2, 421–431, 2014.
15. Wang, R., L. Brönn, S. Gerber, and P. Tlali, "An axial flux magnetically geared permanent magnet wind generator," *IEEJ Transactions on Electrical and Electronic Engineering*, Vol. 10, S123–S132, 2015.
16. Jian, L., K. Chau, and J. Jiang, "A magnetic-geared outer-rotor permanent-magnet brushless machine for wind power generation," *IEEE Transactions on Industry Applications*, Vol. 45, No. 3, 954–962, 2009.
17. Tlali, P., S. Gerber, and R. Wang, "Optimal design of an outer-stator magnetically geared permanent magnet machine," *IEEE Transactions on Magnetics*, Vol. 52, No. 2, 1–10, 2016.